201308001A

厚生労働科学研究費補助金
医療機器開発推進研究事業

循環腫瘍細胞観察可能なナノ粒子質量顕微鏡開発に関する研究

平成25年度　総括研究報告書

研究代表者　瀬藤　光利

平成26（2014）年4月

目　　次

厚生労働科学研究費補助金（医療機器開発推進研究事業）　総括研究報告書

循環腫瘍細胞観察可能なナノ粒子質量顕微鏡開発に関する研究

研究代表者　浜松医科大学・解剖学講座・細胞生物学分野　教授　瀬藤光利

研究要旨

がんが進展するごく早期から血中に存在する循環腫瘍細胞の質的評価は診断・治療に重要である。本研究は、ナノ粒子等を補助剤として活用し、循環腫瘍細胞の質的評価を可能とするための質量顕微鏡を開発することを目的とする。本事業年度は医薬品医療機器総合機構・医療機器戦略相談を利用し、新規医療機器として質量顕微鏡を開発・確立するための方針や方法に関して助言を受けた。そこで機器開発のためには臨床的有用性を持つことが重要であるとの助言を得たことから、乳がん患者末梢血から得られた循環腫瘍細胞の質量顕微鏡解析と網羅的データ解析を行い、病態評価因子との関連性を示す代謝物を質量顕微鏡の循環腫瘍細胞観察によって評価できることを示した。この結果、ナノ粒子等を補助剤として活用した循環腫瘍細胞観察可能な質量顕微鏡が開発された。

研究分担者氏名・所属研究機関名及び所属研究機関における職名

瀬藤光利　浜松医科大学・解剖学講座・細胞生物学分野　教授

池上浩司　浜松医科大学・解剖学講座・細胞生物学分野　准教授

早坂孝宏　浜松医科大学・解剖学講座・細胞生物学分野　特任助教

木村芳滋　浜松医科大学・解剖学講座・細胞生物学分野　特任助教

A．研究目的

厚生労働行政においてがん対策及びがん研究の推進は重要な位置を占める。がんの早期診断、予後判定、治療効果判定はいずれも重要な課題であり、その方法が種々議論され開発されてきた。転移に関する分子メカニズムの解明は、これらいずれの課題にも極めて重要な解決の糸口となりうるテーマである。転移に関しては、従来考えられてきたよりもごく早い病期のうちから、がん細胞が血液中に流れ出し、やがて多臓器に生着し転移巣を形成するというモデルが新規に提唱され注目を集めている。この血液中に存在する腫瘍細胞は循環腫瘍細胞と呼ばれ、検出個数と予後の悪さには正の相関関係があることが報告されている。一方で循環腫瘍細胞の質的な評価に関しては細胞表面マーカーや遺伝子発現に着目した報告が行われているのみであり、評価方法は未だ十分に確立されていない。本研究はこの評価方法を確立し病理診断に応用するために、ナノ粒子等を補助剤として活用した一細胞レベルの超高解像度解析能を備えた循環腫瘍細胞観察可能な質量顕微鏡の開発を目的とする。

質量顕微鏡は研究代表者らが開発してきた質量分析手法であり、生体試料を直接的に二次元質量分析することにより、試料組織上生体物質の種類、位置、相対量を解析する手法である。循環腫瘍細胞観察可能な質量顕微鏡が医療分析機器ジャンルとして成立すれば、国内医療機器産業の振興につながり国内経済にも好影響を及ぼすことが期待できる。

本研究では、循環腫瘍細胞の新規な質的評価方法として用いることのできる一細胞質量顕微鏡法を開発する。質量顕微鏡法ではナノ粒子等を補助剤として用いることにより多くの分子種が観察できることを、研究代表者らは証明してきた。本研究では、新たな循環腫瘍細胞解析機器の確立を目指すために、担がん患者検体から循環腫瘍細胞を回収し統合的解析を行う。末梢血および比較試料である原発巣組織の主な採取対象として乳がんを設定する。乳がんは女性特有のがんであり、中年齢層における発症が少なくないことから、本研究は厚生労働行政の目指す「女性特有のがん対策の推進」及び「働く世代のがん対策」に貢献すると考えられる。

本事業年度は、臨床検体を用いた循環腫瘍細胞の解析を継続し、質量顕微鏡によって得られた測定データと病態評価因子の関連性について解析することにより、質量顕微鏡の臨床的有用性を調べた。

B．研究方法

医薬品医療機器総合機構（PMDA）の薬事戦略相談において本事業のこれまでの結果を提示して助言を受けて、本事業年度の研究方法を策定した。開発される新規医療機器は臨床的有用性を持つことが重要であるとの助言を得たことから、質量顕微鏡の臨床的有用性を調べるため、1) 担がん患者検体の収集、2) 臨床検体の質量顕微鏡解析、3) 病態評価因子と質量顕微鏡解析データ間での関連性の分析、を行なった。

1) 担がん患者検体の収集

臨床検体の取得にあたっては、浜松医科大学乳腺外科および浜松医療センター乳腺外科で、診断もしくは治療を目的として組織採取を行う乳がん患者を対象とした。脂質解析に関する結果の比較対象として、骨髄腫検体測定による得られるデータも活用した。十分なインフォームドコンセントの後、同意の得られた患者から、生検組織採取とともに循環腫瘍細胞採取のため末梢血の採血を行なった。本事業年度は、予算継続審査の際に評価委員より提示されたコメントに従い、対象疾患として乳がんを優先した。収集検体の背景情報は、研究協力者の所属施設において連結可能匿名化の上管理した。

2) 臨床検体の質量顕微鏡解析

試料の回収と解析にあたっては、本課題において昨年度までに新規に創出された、インジウム酸化スズ—MAS コーティングスライドグラス（ITO-MAS コートスライドグラス）を用いた。

循環腫瘍細胞の選択の基本手法としては、全体計画の通り磁気細胞分離法とフローサイトメトリー法を利用した。測定対照として乳がん細胞株 SKBR-3 およびヒト骨髄腫細胞を使用した。原発巣の単一細胞化には、研究全体計画時に考案した通り、検体組織をメスで小断片化した後に酵素処理する方法を用いた。フローサイトメトリー法により細胞を単離および回収した後、一細胞質量顕微鏡解析した。

3) 病態評価因子と質量顕微鏡解析データ間での関連性の分析

データ解析には専用ソフトウェアである MS Imaging Solution 解析を用いた。各測定領域のデータセットを陰性対照領域のデータセットと統合し、リン脂質のシグナル強度に関して統計有意差を示す測定領域を抽出し、一細胞由来のシグナルを検出した測定領域であると定義した。末梢血中からのソーティング数より少ない検出領域数を示した検体のみを最終的な解析に使用した。抽出された測定領域を統合し、原発巣群—循環腫瘍細胞群間での群間検定、および患者予後で区分した循環腫瘍細胞群の群間検定に用いた。

（倫理面への配慮）

本研究は浜松医科大学の医の倫理審査委員会による承認の下に遂行された。該当する患者に当研究に関して患者用説明文書を用い、研究への協力の可否が治療の質に影響しないこと、研究への協力が危険を伴わないこと、研究協力者及び家族の意思を第一に尊重することを十分に説明し、インフォームドコンセントを得られた場合、文書による同意書を得て、疫学研究に関する倫理指針（平成１６年文部科学省・厚生労働省告示第２号）および臨床研究に関する倫理指針（平成１６年厚生労働省告示第４５９号）に厳正に則り研究を施行した。試料は連結可能匿名化を行い情報管理者が適切に管理した。

C．研究結果

1) 担がん患者検体の収集

本事業年度は、対象疾患として乳がんを優先するとともに、ヒト末梢血及び原発巣検体収集も行なった。平成 25 年度の取得検体数は末梢血 32 検体、原発巣 15 検体であった。また、脂質解析に関する結果の比較対象として、骨髄腫患者から末梢血及び骨髄検体を採取し、同様の解析を行なった。検体数は末梢血 1 検体、骨髄 3 検体であった。

2) 臨床検体の質量顕微鏡解析

松浪硝子工業株式会社との共同研究により解析用素材として新たに開発された ITO-MAS コートスライドグラスの製品としての普及を進めた。このスライドグラスは、松浪硝子工業株式会社より販売品目 SI0020M および SI0100M として販売されている。

原発巣・循環腫瘍細胞間の脂質組成比較に際し、引き続き多施設からの検体供与を継続し、平成 25 年度はデータ解析に供する検体数を増やした。

3) 病態評価因子と質量顕微鏡解析データ間での関連性の分析

CD326 陽性、CD45 陰性循環腫瘍細胞の質量顕微鏡解析を行い、MS Imaging Solution 解析ソフトウェアにより原発巣検体試料に由来する細胞の質量顕微鏡法解析結果との比較を行なった。ホスファチジルコリン（PC）（32:4）に相当する質量電荷比（*m/z*）748.5 が循環腫瘍細胞において原発巣の 2.0 倍の平均シグナル強度を示すことを明らかにした。さらに患者予後を代表する因子として採血時点で病態コントロール可能な状態であったかどうかを指標として患者を予後良好群・予後不良群の 2 群に分類したときに、PC（34:3）に相当する *m/z* 794.5 が予後良好群において予後不良群の 1.7 倍の平均シグナル強度を示すことを明らかにした。これらのことから、PC（32:4）及び PC(34:3)を病態や患者予後と関連する循環腫瘍細胞の新たな質的評価軸を質量顕微鏡によって示すことが可能となった。また、比較対象として実施した骨髄腫患者検体を用いた一細胞解析においては、末梢血中骨髄腫細胞対骨髄腔内骨髄腫細胞間の比較を行い、骨髄腔内細胞に比べ末梢血中細胞ではパルミチン酸の検出量が大きい傾向にあることを見出した。骨髄腫細胞の由来の違いを質量顕微鏡によって示

すことが可能となった。

D．考察

1) 担がん患者検体の収集

他施設と連携し症例の収集を継続し、目標検体数である80検体を上回る合計108検体の収集を達成することができた。収集された検体から循環腫瘍細胞及び原発巣の分子プロファイルを取得し、臨床情報と質量顕微鏡解析結果の統合的解析に結びつけることができた。

2) 臨床検体の質量顕微鏡解析

循環腫瘍細胞の定義領域のバックグラウンドノイズのより少ないものへと変更させ、安定的な解析手法として固定した。ITO-MASコートスライドグラスは、本研究課題においてナノ粒子等を補助剤として活用する循環腫瘍細胞の質量顕微鏡解析に適した新たな素材を探索する中で創出され、循環腫瘍細胞の高効率での回収と高感度測定に有用に機能した。本事業年度を通して一般販売まで漕ぎ付けることができた。今後も一細胞解析を始めとする微量サンプルの質量顕微鏡解析に広く用いられることが期待される。

3) 病態評価因子と質量顕微鏡解析データ間での関連性の分析

乳がん循環腫瘍細胞の質量顕微鏡解析によって、循環腫瘍細胞を質的に評価するための分子として、PC（32:4）、PC（34:3）が発見された。中でもPC（34:3）は患者病態と関連する新規分子マーカーであることから、循環腫瘍細胞の質量顕微鏡を用いた解析の臨床的有用性が示された。また、骨髄腔中の骨髄腫細胞細胞膜において、末梢血に比べてパルミチン酸含有量が少ない傾向を示すことが、質量顕微鏡を用いることによって可能となった。このことは質量顕微鏡が種類の異なる複数のがんの観察が可能であることを示している。

E．結論

乳がん患者の原発巣と末梢血から採取された細胞を材料として質量顕微鏡解析を行い、原発巣と循環腫瘍細胞において異なるシグナル強度を示す代謝物を明らかにすることができた。この結果、これまで個数のみで評価されていた循環腫瘍細胞を質的に評価することが質量顕微鏡によって可能となった。この結果、ナノ粒子等を補助剤として活用した循環腫瘍細胞観察可能な質量顕微鏡が開発された。

F．健康危険情報

本事業年度、特に健康危険情報として報告すべきものはなかった。

G．研究発表

1．論文発表

【原著論文】

(1) Ide Y, Waki M, Ishizaki I, Nagata Y, Yamazaki F, Hayasaka T, Masaki N, Ikegami K, Kondo T, Shibata K, Ogura H, Sanada N, Setou M. Single Cell Lipidomics of SKBR-3 Breast Cancer Cells by Using Time-of-Flight Secondary-Ion Mass Spectrometry. Surf Interface Anal. in press.

(2) Nagata Y, Ishizaki I, Waki M, Ide Y, Hossen A, Ohnishi K, Sanada N, Setou M. Glutaraldehyde Fixation Method for Single-Cell Lipid Analysis by Time-of-Flight Secondary Ion-Mass Spectrometry. Surf Interface Anal. in press.

(3) Uchiyama Y, Hayasaka T, Masaki N, Watanabe Y, Masumoto K, Nagata T, Katou F, Setou M. Imaging mass spectrometry distinguished the cancer and stromal regions of oral squamous cell carcinoma by visualizing phosphatidylcholine (16:0/16:1) and phosphatidylcholine (18:1/20:4). Anal Bioanal Chem. 2014 Feb;406(5):1307-16. doi: 10.1007/s00216-013-7062-3. Epub 2013 Jun 1.

(4) Ide Y, Waki M, Hayasaka T, Nishio T, Morita Y, Tanaka H, Sasaki T, Koizumi K, Matsunuma R, Hosokawa Y, Ogura H, Shiiya N, Setou M. Human Breast Cancer Tissues Contain Abundant Phosphatidylcholine(36:1) with High Stearoyl-CoA Desaturase-1 Expression. PLoS One. 2013 Apr 16;8(4):e61204. doi:10.1371/journal.pone.0061204. Print 2013.

(5) Morita Y, Sakaguchi T, Ikegami K, Goto-Inoue N, Hayasaka T, Hang VT, Tanaka H, Harada T, Shibasaki Y, Suzuki A, Inaba K, Murakami M, Setou M, Konno H. Lysophosphatidylcholine acyltransferase 1 altered phospholipid composition and regulated hepatoma progression. J Hepatol. 2013 Aug;59(2):292-9. doi: 10.1016/j.jvs. 2013.01.030. Epub 2013 Apr 6.

【和文総説】

(1) 佐野圭吾、瀬藤光利、質量顕微鏡法を用いた生体組織解析、医学書院「生体の科学」、2013年12月64巻6号p614-620

(2) 松下祥子、瀬藤光利、質量顕微鏡を用いた医薬研究の発展、ファルマシア、2013年12月49巻12号 p1159-1163

(3) 佐野圭吾、瀬藤光利、走査型レーザーイオン化による生体組織の質量イメージング、日本光学会(応用物理学会)、2013年11月42巻11号p555-561

(4) 稲見勝朗、瀬藤光利、顕微鏡と画像データ処理：質量顕微鏡、ぶんせき、2013年第8号p470-471

(5) 早坂孝宏、瀬藤光利、質量顕微鏡を用いたホメオスタシス破綻の可視化、The Lipid、2013

年 7 月 24 巻 3 号 p4-11

【英文著書】

(1) Waki M, Sugiyama E, Kondo T, Sano K, Setou M. Nanoparticle-Assisted Laser Desorption/Ionization for Metabolite Imaging. Methods Mol Biol. in press.

【和文著書】

(1) 永田泰之、井手佳美、瀬藤光利、最新生理活性脂質研究-実験手法、基礎的知識とその応用-（第 1 章）技術編　質量顕微鏡　遺伝子医学 MOOK、2013 年、24 号 p71-76.
(2) 近藤豪、瀬藤光利、医用質量分析ガイドブック　疾患のイメージング質量分析、診断と治療社、2013 年 12 月 25 日 p121-126

2. 学会発表

(1) 井手佳美、脇紀彦、小倉廣之、瀬藤光利、1 価不飽和脂肪酸を含むホスファチジルコリンが乳癌癌部に高集積する　質量顕微鏡法による乳癌脂質解析、第 72 回日本癌学会、横浜、2013 年 10 月
(2) Yoshimi Ide, Michihiko Waki,Itsuko Ishizaki, Yasuyuki Nagata, Hiroyuki Ogura, Noriaki Sanada and Mitsutoshi Setou 、 Single-Cell Analysis of Human Breast Cancer Cells by Secondary-Ion Mass Spectrometry 、 19th International Conference on Secondary Ion Mass Spectrometry、韓国、2013 年 9 月
(3) Yasuyuki Nagata, Itsuko Ishizaki, Yoshimi Ide, Michihiko Waki, Kazunori Ohnishi, Noriaki Sanada and Mitsutoshi Setou、Single Cell Analysis of Multiple Myeloma With Secondary Ion Mass Spectrometry、19th International Conference on Secondary Ion Mass Spectrometry、韓国、2013 年 9 月
(4) 永田　泰之、石崎　逸子、井手　佳美、脇　紀彦、大西　一功、眞田　則明、瀬藤　光利、多発性骨髄腫細胞における脂肪酸組成の変化、日本医用マススペクトル学会、神戸、2013 年 9 月
(5) 瀬藤光利、細胞・組織の２Ｄ質量分析イメージング、日本学術会議公開シンポジウム「医学・生命科学の革新的発展に資する統合バイオイメージングの展望」、東京、2013 年 9 月
(6) 瀬藤光利、創薬における質量顕微鏡法の可能性、創薬薬理フォーラム 第 21 回シンポジウム、東京、2013 年 9 月
(7) Mitsutoshi Setou 、 Advanced Applications of Imaging Mass Spectrometry in Clinical Research、Imaging Mass Spectrometry Workshop、韓国、2013 年 7 月
(8) 瀬藤光利、質量顕微鏡研究とトランスレーショナルリサーチャー、第 21 回日本乳癌学会学術総会、浜松、2013 年 6 月

H．知的財産権の出願・登録状況

1. 特許取得

(1) 出願番号：2013-177105　出願日：2013/8/28
タイトル：骨髄腫細胞死誘導剤及びこれを含有する骨髄腫治療用医薬組成物、発明人：永田泰之、瀬藤光利

2. 実用新案登録

該当なし

3.その他

該当なし

研究成果の刊行に関する一覧表

雑誌【原著論文】

発表者氏名	論文タイトル名	発表誌名	巻号	ページ	出版年
Ide Y, Waki M, Ishizaki I, Nagata Y, Yamazaki F, Hayasaka T, Masaki N, Ikegami K, Kondo T, Shibata K, Ogura H, Sanada N, Setou M.	Single Cell Lipidomics of SKBR-3 Breast Cancer Cells by Using Time-of-Flight Secondary-Ion Mass Spectrometry.	Surf Interface Anal.	in press.	in press.	2014
Nagata Y, Ishizaki I, Waki M, Ide Y, Hossen A, Ohnishi K, Sanada N, Setou M.	Glutaraldehyde Fixation Method for Single-Cell Lipid Analysis by Time-of-Flight Secondary Ion-Mass Spectrometry.	Surf Interface Anal.	in press.	in press.	2014
Uchiyama Y, Hayasaka T, Masaki N, Watanabe Y, Masumoto K, Nagata T, Katou F, Setou M.	Imaging mass spectrometry distinguished the cancer and stromal regions of oral squamous cell carcinoma by visualizing phosphatidylcholine (16:0/16:1) and phosphatidylcholine (18:1/20:4).	Anal Bioanal Chem.	406(5)	1307-16	2014
Ide Y, Waki M, Hayasaka T, Nishio T, Morita Y, Tanaka H, Sasaki T, Koizumi K, Matsunuma R, Hosokawa Y, Ogura H, Shiiya N, Setou M.	Human Breast Cancer Tissues Contain Abundant Phosphatidylcholine(36:1) with High Stearoyl-CoA Desaturase-1 Expression.	PLoS One.	8(4)	e61204	2013
Morita Y, Sakaguchi T, Ikegami K, Goto-Inoue N, Hayasaka T, Hang VT, Tanaka H, Harada T, Shibasaki Y, Suzuki A, Inaba K, Murakami M, Setou M, Konno H.	Lysophosphatidylcholine acyltransferase 1 altered phospholipid composition and regulated hepatoma progression.	J Hepatol.	59(2)	292-9	2013

雑誌【和文総説】

発表者氏名	論文タイトル名	発表誌名	巻号	ページ	出版年
佐野圭吾、瀬藤光利	質量顕微鏡法を用いた生体組織解析	医学書院「生体の科学」	64巻6号	p614-620	2013
松下祥子、瀬藤光利	質量顕微鏡を用いた医薬研究の発展	ファルマシア	49巻12号	p1159-1163	2013
佐野圭吾、瀬藤光利	走査型レーザーイオン化による生体組織の質量イメージング	日本光学会(応用物理学会)	42巻11号	p555-561	2013
稲見勝朗、瀬藤光利	顕微鏡と画像データ処理：質量顕微鏡	ぶんせき	第8号	p470-471	2013
早坂孝宏、瀬藤光利	質量顕微鏡を用いたホメオスタシス破綻の可視化	The Lipid	24巻3号	p4-11	2013

書籍【英文著書】

著者氏名	論文タイトル名	書籍全体の編集者名	書　籍　名	出版社名	出版地	出版年	ページ
Waki M, Sugiyama E, Kondo T, Sano K, Setou M.	Nanoparticle-Assisted Laser Desorption/Ionization for Metabolite Imaging.	Walker, John M.	Methods Mol Biol.	Springer	ドイツ	2014	in press.

書籍　【和文著書】

著者氏名	論文タイトル名	書籍全体の編集者名	書　籍　名	出版社名	出版地	出版年	ページ
永田泰之、井手佳美、瀬藤光利	最新生理活性脂質研究-実験手法、基礎的知識とその応用-　(第１章) 技術編　質量顕微鏡	青木淳賢、杉本幸彦、村上誠	遺伝子医学MOOK	株式会社メディカルドゥ	日本	2013	p71-76
近藤豪、瀬藤光利	疾患のイメージング質量分析	丹羽利充、野村文夫	医用質量分析ガイドブック	診断と治療社	日本	2013	p121-126

Anal Bioanal Chem
DOI 10.1007/s00216-013-7062-3

ORIGINAL PAPER

Imaging mass spectrometry distinguished the cancer and stromal regions of oral squamous cell carcinoma by visualizing phosphatidylcholine (16:0/16:1) and phosphatidylcholine (18:1/20:4)

Yoshiyuki Uchiyama · Takahiro Hayasaka · Noritaka Masaki · Yoshiko Watanabe · Kazuma Masumoto · Tetsuji Nagata · Fuminori Katou · Mitsutoshi Setou

Received: 14 November 2012 / Revised: 22 April 2013 / Accepted: 10 May 2013
© Springer-Verlag Berlin Heidelberg 2013

Abstract Most oral cancers are oral squamous cell carcinoma (OSCC). The anatomical features of OSCC have been histochemically evaluated with hematoxylin and eosin. However, the border between the cancer and stromal regions is unclear and large portions of the cancer and stromal regions are resected in surgery. To reduce the resected area and maintain oral function, a new method of diagnosis is needed. In this study, we tried to clearly distinguish the border on the basis of biomolecule distributions visualized by imaging mass spectrometry (IMS). In the IMS dataset, eleven signals were significantly different in intensity ($p<0.01$) between the cancer and stromal regions. Two signals at m/z 770.5 and m/z 846.6 were distributed in each region, and a clear border was revealed. Tandem mass spectrometric (MS/MS) analysis identified these signals as phosphatidylcholine (PC) (16:0/16:1) at m/z 770.5 in the cancer region and PC (18:1/20:4) at m/z 846.6 in the stromal region. Moreover, the distribution of PC species containing arachidonic acid in the stromal region suggests that lymphocytes accumulated in response to the inflammation caused by cancer invasion. In conclusion, the cancer and stromal regions of OSCCs were clearly distinguished by use of these PC species and IMS analysis, and this molecular identification can provide important information to elucidate the mechanism of cancer invasion.

Keywords Imaging mass spectrometry (IMS) · Oral cancer · Phosphatidylcholine · Palmitic acid · Arachidonic acid · Matrix-assisted laser-desorption ionization (MALDI)

Introduction

Most cases of head and neck cancer are oral cancers of the tongue, floor of the mouth, gingiva, or salivary glands. Oral cancers are histologically classified as squamous cell carcinomas (SCCs), adenoid cystic carcinoma, or mucoepidermoid. Oral SCCs (OSCCs) account for more than 80 % of all head and neck cancers and are fatal without surgical resection. The extent of cancer is evaluated by a combination invasive biopsies and differentiation on the basis of several criteria, for example the Jakobsson classification [1], the Anneroth classification [2], and the Yamamoto–Kohama classification [3]. Moreover, the surgeon's experience determines the margin area resected in the stromal region. The stromal region includes the connective tissue area around the cancer lesion, unlike normal tissue. It is known that lymphocyte immune cells are found in the stromal region. The resected tissue is histochemically analyzed and the completeness of resection is judged. However, there is a dangerous possibility of cancer cells remaining because it is very difficult to resect all the cancer in the narrow oral space. If cancer cells remain in the oral

Published in the topical collection *Biomedical Mass Spectrometry* with guest editors Mitsutoshi Setou, Toshimitsu Niwa, and Akira Ishii.

Y. Uchiyama · Y. Watanabe · K. Masumoto · T. Nagata · F. Katou
Department of Oral and Maxillofacial Surgery,
Hamamatsu University School of Medicine,
1-20-1 Handayama, Higashi-ku,
Hamamatsu, Shizuoka 431-3192, Japan

T. Hayasaka · N. Masaki · M. Setou (✉)
Department of Cell Biology and Anatomy, Hamamatsu University School of Medicine, 1-20-1 Handayama, Higashi-ku,
Hamamatsu, Shizuoka 431-3192, Japan
e-mail: setou@hama-med.ac.jp

Published online: 01 June 2013

Imaging mass spectrometry (IMS)

Tissue section preparation

Tissues blocks were sectioned at −20 °C, by use of a cryostat (CM 1950; Leica, Wetzler, Germany), to a thickness of 8 μm in the direction of the long axis, as described elsewhere [24, 25]. To prevent degradation of mass spectra in IMS analysis, OSCC blocks were not embedded in OCT polymer during this procedure [25]. The frozen sections were thaw-mounted on indium–tin oxide (ITO)-coated glass slides (Bruker Daltonics) and stored at −20 °C until used for IMS analysis.

Spray coating of the matrix solution

A DHB solution (50 mg mL^{-1} DHB and 10 mmol L^{-1} potassium acetate in 70 % methanol, 1 mL) was used as the matrix [26]. The potassium salt can help to ionize molecules in the form $[M + K]^+$, without $[M + H]^+$ and $[M + Na]^+$, in positive-ion mode, making analysis of the mass spectrum fairly easy. The matrix solution was sprayed on to the sample sections by use of a 0.2-mm nozzle caliber airbrush (Procon Boy FWA Platinum; Mr Hobby, Tokyo, Japan).

IMS conditions

IMS was performed by use of a MALDI–TOF–TOF-type instrument (Ultraflex II TOF/TOF; Bruker Daltonics). This instrument was equipped with a 355-nm Nd:YAG laser. The ionized molecules were detected in the positive reflectron mode by using an external calibration method. Mono DHB ($[M + H]^+$, *m/z* 155.03) and human angiotensin II ($[M + H]^+$, *m/z* 1,046.54) were used for calibration. Mass spectra were acquired in the mass range *m/z* 400–1,200. The laser energy and detector gain were optimized to maximize the sensitivity of signal detection in the IMS analysis. Raster scans on tissue surfaces were performed automatically by use of flexControl and flexImaging 2.1 software (Bruker Daltonics). The number of laser irradiations was 200 shots in each spot. The distance between data points was 100 μm. Image reconstruction was performed by use of flexImaging 2.1 software.

IMS data analysis

The regions of interest (ROIs) in the cancer and stromal regions were defined by reference to the HE staining in adjacent sections. The IMS data format of the flexImaging 2.1 software was converted into Analyze 7.5 file format to statistically analyze the IMS data by use of SIMtool software (in-house software; Shimadzu, Kyoto, Japan). With the exception of isotope peaks, all peaks were picked up from ROIs that were defined as "cancer region" or "stromal region", and these distributions were visualized on a tissue section. These signal intensities between the cancer and stromal regions were statistically assessed by use of Welch's *t*-test, and *p*-values <0.01 were regarded as significant. Finally, the peaks with significant differences were applied to four other datasets and visualized as ion images.

MS/MS analysis

Because multiple fatty acid isobars are possible, the MS/MS analysis was performed on tissue sections in the positive-ion mode by use of the QSTAR Elite System (Applied Biosystems/MDS Sciex, Foster City, CA, USA), a hybrid quadrupole–TOF mass spectrometer equipped with an orthogonal MALDI source and a pulsed Nd:YAG laser. The laser energy and collision energy were optimized to maximize the sensitivity of signal detection in the MS/MS analysis. Biomolecules were identified by referring to the results of a Metabolite MS Search (http://www.hmdb.ca/spectra/ms/search)

Results

HE staining of OSCC specimens from case 1

Frozen specimens of OSCC were obtained from gingiva on which no preoperative therapy had been performed. To analyze the morphological features in detail, we used HE staining. The HE-stained section from case 1 is shown in Fig. 1. In Fig. 1a, the epidermal layer is on the upper side and the lamina propria is on the bottom. The cancer was found on the left side, and the histopathological diagnosis of this OSCC was well-differentiated. An enlarged view of the typical cancer region is shown in Fig. 1b. Here, the cancer nests (i.e., clusters of carcinoma cells) are remarkable. Invasion of the cancer from an epidermal layer to the lamina propria can be observed. Cancer cells were observed in connective tissue areas around the cancer nests and were referred to as the "cancer stroma". An enlarged view of a cancer-free stromal region is shown in Fig. 1c (the right side in Fig. 1a). The stromal region includes the connective tissue area around the cancer lesion, unlike normal tissue. Lymphocyte immune cells accumulated in the stromal regions of OSCC tissue from case 1. By use of HE staining the cancer and stromal regions were almost distinguished. However, a more precise border was needed to reduce the resection area. Therefore, we next applied the IMS technique to an adjacent tissue section.

Comparison of the mass spectra in each region and ion images from case 1

After acquiring the IMS dataset, the average mass spectra from each region were created in the mass range *m/z* 400–1,200 (inset in Fig. 2a, b). First, with the exception of isotope

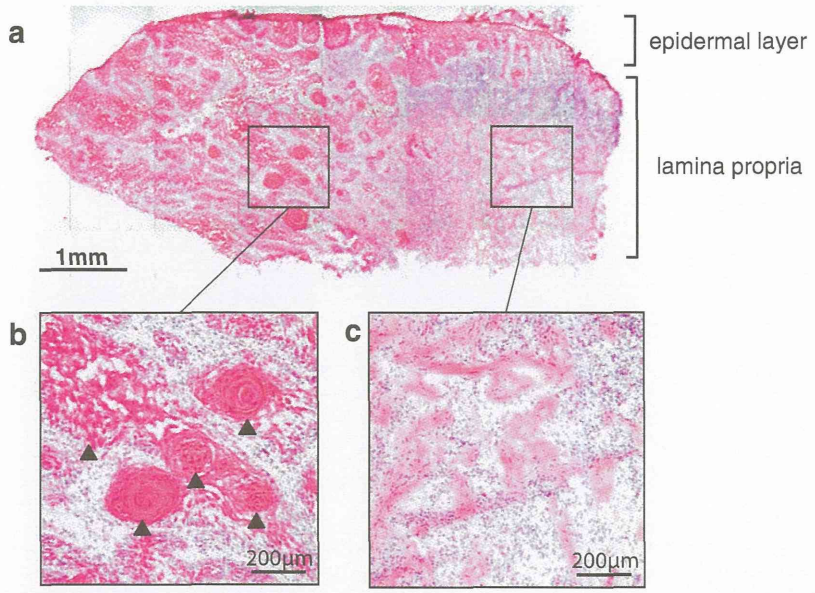

Fig. 1 HE-stained tissue of oral squamous cell carcinoma (OSCC) of the maxillary gingiva from case 1. **a** An overall view from a continuous frozen section. The cancer region is located *on the left* and the stromal region is located *on the right*. Invasion from an epidermal layer to the lamina propria is observed in the cancer region. The border between the cancer region and the stromal region is indistinct, and cancer cells and connective tissue are mixed. **b** Cancer nests (*arrow*) and cancer stroma are observed in the cancer region. Cancer nests were clusters of carcinoma cells, and the cancer stroma consisted of connective tissue areas around the cancer nests. **c** The stromal region shows the neoplasm, indicating connective tissue areas around the cancer region

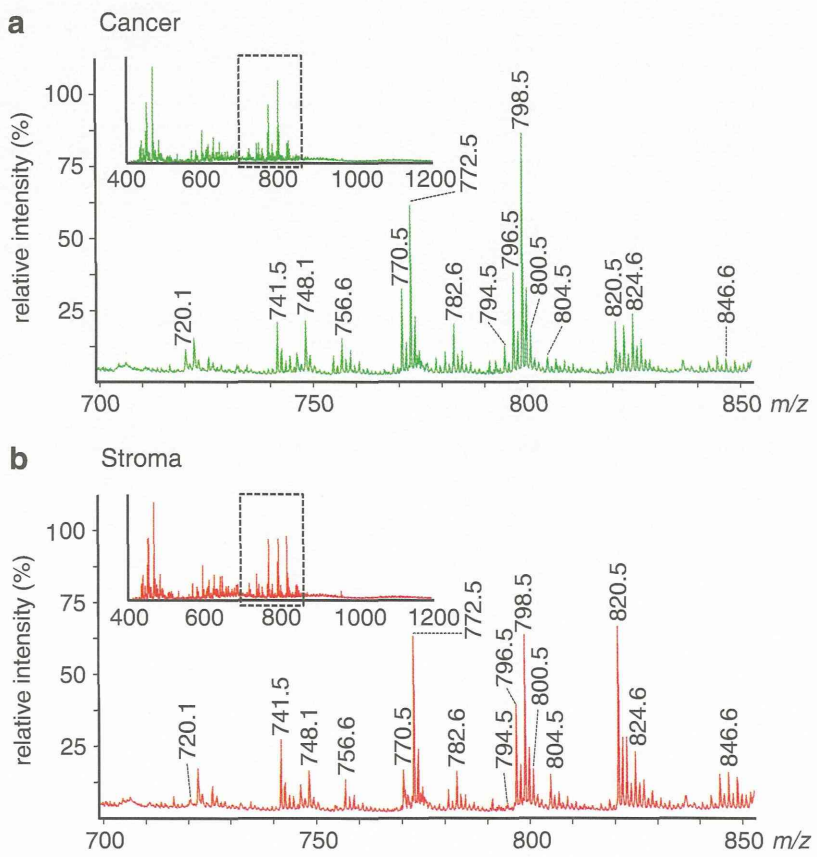

Fig. 2 Comparison of mass spectra from the cancer and stromal regions from case 1. **a** The average mass spectrum from the cancer region was obtained in the range *m/z* 400–1,200 (*inset*). The mass spectrum was extracted in the range *m/z* 700–850. **b** In the same way, the average mass spectrum from the stromal region was obtained in the ranges *m/z* 400–1,200 (*inset*) and *m/z* 700–850. The characteristic peaks were compared between the cancer and stromal regions. Each *labeled number* shows a peak of characteristic signal intensity in a cancer region. The relative intensity was based on a peak with maximum intensity in each region. All peaks were observed in common in each mass spectrum, but some of the peaks had different intensities

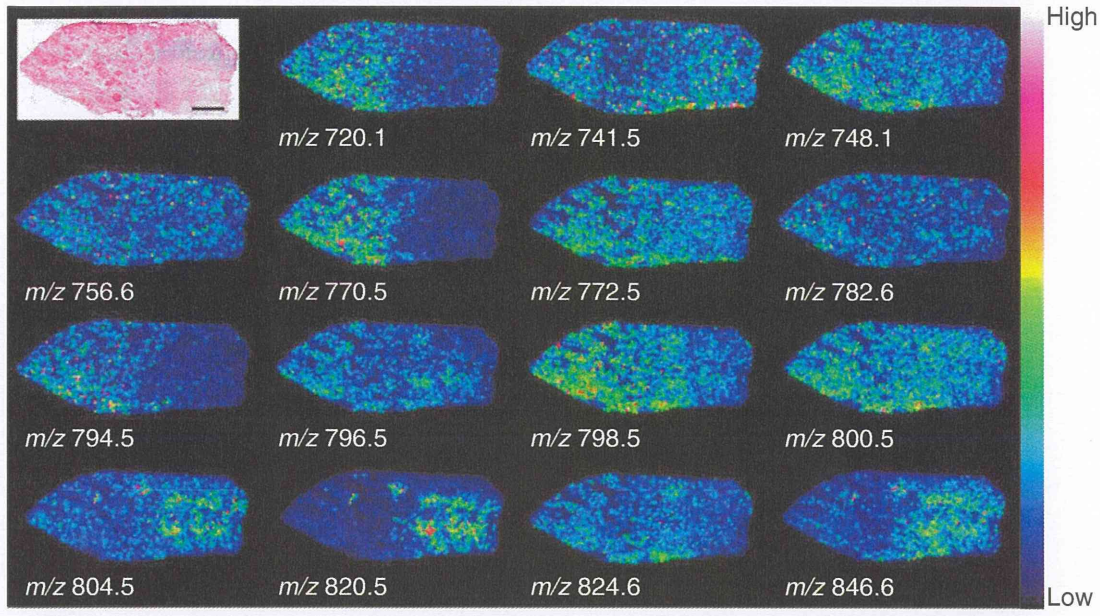

Fig. 3 Ion images of the top 15 signals from case 1. The *threshold of the color scale* was adjusted in each ion image to show the clear distribution. The ions *m/z* 720.1, 770.5, and 794.5 were clearly distributed in the cancer region. In contrast, the ions *m/z* 804.5, 820.5, and 846.6 were distributed in the stromal region. Other signals were distributed over the whole region

Table 1 Molecular screening using Welch's *t*-test

m/z	Signal intensity (a.u.)		*p*-value
	Cancer	Stroma	
770.5	27.8 ± 0.9	7.1 ± 0.2	1.60×10^{-78}
820.5	14.6 ± 0.5	53.9 ± 1.9	2.70×10^{-68}
846.6	5.1 ± 0.2	12.4 ± 0.4	1.73×10^{-62}
794.5	10.2 ± 0.3	3.7 ± 0.1	1.51×10^{-59}
720.1	8.3 ± 0.3	4.4 ± 0.1	2.44×10^{-38}
804.5	5.7 ± 0.2	11.4 ± 0.4	1.58×10^{-33}
741.5	14.8 ± 0.5	22.3 ± 0.8	2.56×10^{-16}
798.5	69.4 ± 2.0	52.2 ± 1.5	2.15×10^{-11}
748.1	16.6 ± 0.5	13.1 ± 0.4	1.31×10^{-7}
782.6	14.9 ± 0.4	12.5 ± 0.4	2.67×10^{-5}
756.6	11.5 ± 0.4	10.0 ± 0.3	1.13×10^{-3}

Eleven molecules were significantly different ($p<0.01$) between the cancer and stromal regions. The shaded signal intensities were significantly higher than their counterparts in the cancer or stromal region

peaks, the top 80 peaks were acquired in the mass range *m/z* 400–1,200 by use of SIMtool software. In the *m/z* ranges 400–700 and 850–1,200, small differences in signal intensity were observed for 65 peaks in each region. In contrast, differences in signal intensity were observed for 15 peaks in the *m/z* 700–850 range. It is known that this mass range corresponds to phospholipid species in positive-ion mode. The 15 signals, which were *m/z* 720.1, 741.5, 748.1, 756.5, 770.5, 772.5, 782.6, 794.5, 796.5, 798.5, 800.5, 804.5, 820.5, 824.6, and 846.6, are visualized as ion images in Fig. 3. Different types of distribution were visualized by IMS. The ion images at *m/z* 720.1, 770.5, and 794.5 were clearly distributed in the cancer region, including cancer cells, whereas those at *m/z* 804.5, 820.5, and 846.6 were distributed in the stromal region including lymphocytes and plasma cells. Other signals at *m/z* 741.5, 748.1, 756.5, 772.5, 782.6, 796.5, 798.5, 800.5, and 824.6 were distributed throughout the whole area without significant differences in intensity among regions.

Statistical analysis between cancer and stromal regions from case 1

To clarify significant differences between the cancer and stromal regions from case 1, we used the Welch's *t*-test for the 15 peaks in the mass range *m/z* 700–850. As shown in Table 1, 11 peaks were significantly different ($p<0.01$) between the regions; average signal intensity, standard error, and *p*-value for each *m/z* value are shown. Six molecules in particular, i.e., those associated with the signals *m/z* 720.1, 770.5, 794.5, 804.5, 820.5, and 846.6, were of significantly different intensity in the cancer and stromal regions; these are shown by using averaged signal intensities as a bar graph in Fig. 4. The signals at *m/z* 720.1, 770.5, and 794.5 increased in the cancer region. The signals at *m/z* 804.5, 820.5, and 846.6 increased in stromal region.

Distributions of cancer region-positive and stromal region-positive signals from cases 1–5

We performed IMS analysis on more four cases, cases 2–5, which were well-differentiated and for which accumulation of lymphocytes was observed, much as in case 1, and used the six *m/z* values that were significantly different between the cancer and stromal regions in case 1. These signals are visualized as ion images in Fig. 5. The ion images reconstructed by use of signals at *m/z* 720.1, 770.5, and 794.5 were cancer region-positive. In contrast, the ion images reconstructed by use of the signals at *m/z* 804.5, 820.5, and 846.6 were stromal region-positive. The merged images of *m/z* 770.5 and 846.6 revealed the distribution of the cancer and stromal regions with no overlap and the borders are more clearly visualized than those of the HE-stained section. The *p*-value for *m/z* 820.5 was better than that for *m/z* 846.6, as shown in Table 1. However, the ion distribution was limited to a part

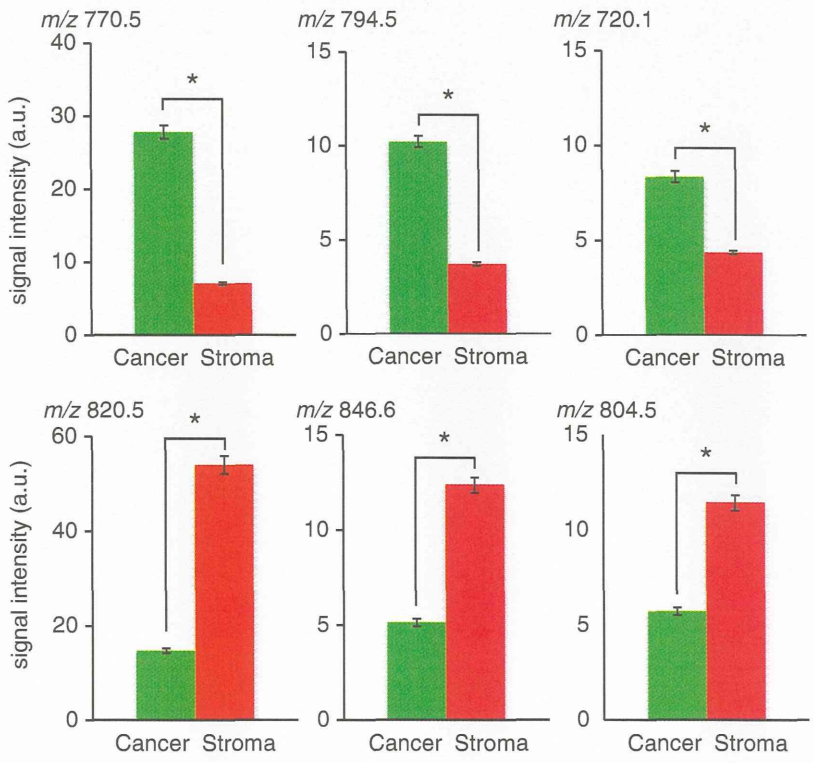

Fig. 4 Statistical analysis between cancer and stromal regions from case 1. Significances of differences in signal intensities in the cancer and stromal regions were determined by use of Welch's *t*-test. The *error bar* represents the standard error. Each of the signals at *m/z* 720.1, 770.5 and 794.5 were increased in cancer regions. Each of the signals at *m/z* 804.5, 820.5, and 846.6 were increased in stromal regions. For all of the *m/z* signals compared here, *p*-values less than 0.01 were obtained; statistical significance is indicated by an *asterisk*

of the stromal region. Therefore, we selected the signal at *m/z* 846.6 as a representative stroma-positive signal.

Molecule identification

MS/MS analysis of tissue sections was performed to identify the structures of the biomolecules evaluated by the statistical analysis. A molecule corresponding to *m/z* 770.5 was assigned to $[PC + K]^+$ because neutral losses of 59 Da (*m/z* 711.4) and 183 Da (*m/z* 587.4) from a precursor ion in the MS/MS spectrum, indicative of a trimethylamine and a choline head group, respectively, were observed (Fig. 6a) [27, 28]. Moreover, the signal at *m/z* 455.1 indicated a neutral loss of 256 Da corresponding to palmitic acid (16:0) from the signal at *m/z* 711.4. The Metabolite MS Search identified a candidate, $[PC (diacyl-32:1) + K]^+$. Therefore, this molecule was identified as $[PC (diacyl-16:0/16:1) + K]^+$. In the same way, a molecule corresponding to *m/z* 846.6 was assigned as $[M + K]^+$ ion of PC (diacyl-18:1/20:4), because neutral losses of 59 Da and 183 Da in the MS/MS spectrum and a neutral loss of 282 Da corresponding to oleic acid (18:1) were also observed (Fig. 6b) [27, 28].

Discussion

This study is the first IMS analysis performed on OSCC tissue, and the first study to compare signals in the cancer and stromal regions. IMS has also been applied to other cancer samples. Morita et al. reported that histone H4 (*m/z* 1,325.6) was found specifically in undifferentiated gastric cancer tissue, after they compared normal tissue and gastric cancer tissues with different degrees of differentiation by IMS [29]. Shimma et al. also reported that SM (d18:1/16:0) at *m/z* 725.4 was specifically distributed in a cancer region by comparing the mass spectrum obtained from colon cancer liver metastasis tissue [22]. Thus, IMS has been proved useful for identification of specific molecules, for example peptides and phospholipids, in cancer regions. In the classification of OSCCs, the criteria for cancer resection in surgery must be modified and reduction of the resection area is needed because resection of a large area sometimes results in a loss of oral function. However, a diagnosis made using HE staining of biopsy tissue does not clearly distinguish between the cancer and stromal region (Fig. 1). Therefore, there has been a need to identify the biomolecules to determine the border between the cancer and

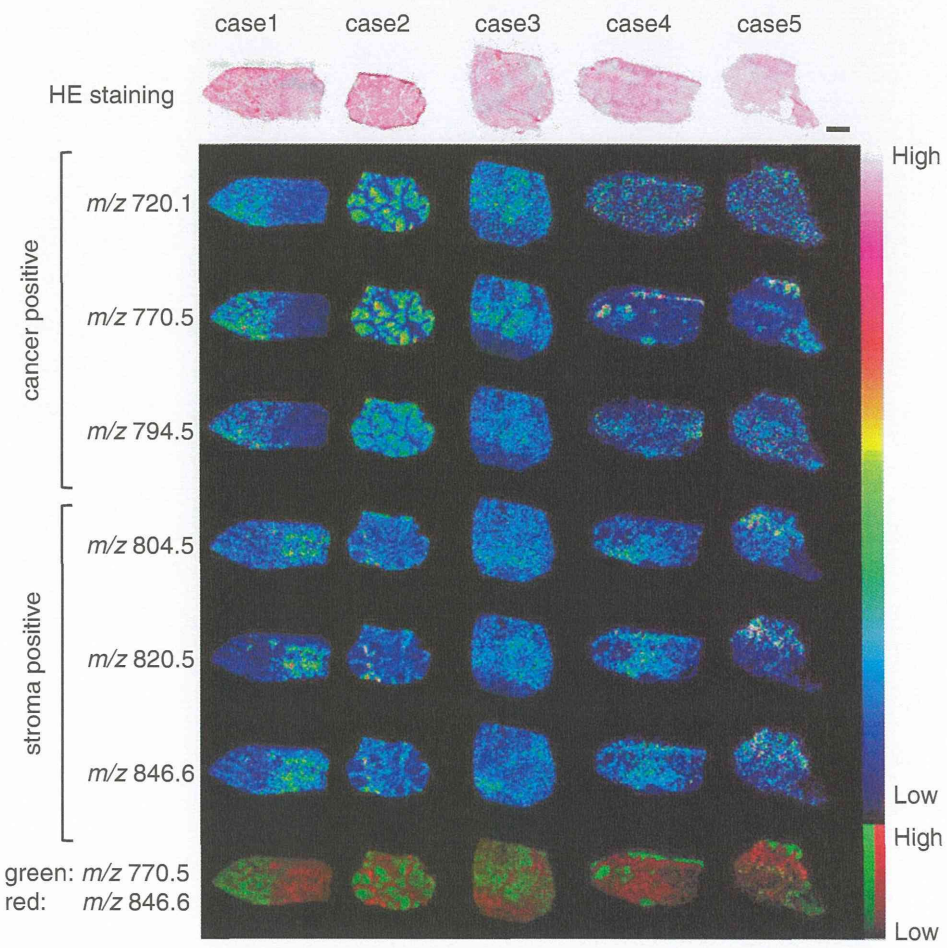

Fig. 5 Ion images with statistically significant differences between the cancer and stromal regions from cases 1–5. We applied six peaks with significantly different intensity to the IMS datasets from cases 2–5 and reconstructed the ion images. The histopathological diagnosis of all cases was well differentiated. Ion images captured cancer-specific distributions at *m/z* 720.1, 770.5, and 794.5. Ion images captured stroma-specific distributions at *m/z* 804.5, 820.5, and 846.6. The merged image from the signal intensities at *m/z* 770.5 and 846.6 revealed the complementary distributions. *Scale bar* = 1 mm

region after surgery, infiltration and metastasis will again result in a serious problem. In general, in cancer tissue intercellular adhesion is weakened, and the motor ability of the cancer cells is enhanced. The cancer cells invade the basal membrane and the membrane disintegrates. The cancer cells are carried in the interstitial connective tissue and metastasize through blood vessels toward other organs. Indeed, the remaining cancer cells induce recrudescence [4]. Finally, OSCCs result in death as a result of infiltration and metastasis. Thus, all cancer cells should be completely resected with a sufficient margin. On the other hand, the margin often prevents the maintenance of oral function. Therefore, criteria for precise surgical resection are needed.

In previous studies, immunological analysis has been applied to OSCC. Cancer growth factors, for example PCNA [5] and Ki-67 [6], have been immunohistologically evaluated to elucidate the extent of tumor invasion in comparison with conventional classification of OSCCs. These proteins have been determined to be biomarkers because of their correlation with the classification. However, these proteins are distributed in normal cells, and it is difficult to determine the minimum margin to be resected in surgery by using the distribution of PCNA and Ki-67. Lipids are also important biological materials, with proteins, nucleic acids, and sugars. Lipids are involved in cell proliferation [7] and differentiation, metabolism control, immunity, and inflammation [8]. The location and metabolism of lipids are believed to be related to the growth of cancer, the invasion of cancer, and the mechanism of metastasis [9, 10]. Brasitus et al. analyzed lipid extract from cells and tissues by thin-layer chromatography and gas chromatography and revealed changes of lipid composition which depended on the development of colon cancer [11]. However, the lipid extract is not suitable for determining the border between the cancer and stromal regions, and thus an imaging technique is needed.

Imaging mass spectrometry (IMS) enables us to visualize the distribution of many biomolecules, without any labeling, in a single analysis, and to identify the biomolecules on a tissue section [12]. The technique is usually applied in the form of secondary mass spectrometry (SIMS) and matrix-assisted laser-desorption ionization (MALDI). SIMS has good resolution for imaging and the resolution is <1 μm. However, the analytes are limited to biomolecules with low molecular weight because those of high molecular weight are fragmented. In contrast, MALDI [13] can ionize biomolecules of high molecular weight, for example proteins [14], lipids [15, 16], nucleic acids [17], and sugars [18], on a tissue section. IMS using MALDI-time-of-flight (TOF) is especially useful for lipid analysis [19, 20] because the technique can separately visualize even the differences between the fatty acid components of lipids [16, 20].

The technique has been applied to several pathology samples, including cancerous tissue, and has revealed the altered phospholipid composition in the diseased region compared with the normal region [21]. Shimma et al. used IMS to examine tissue sections from colon cancer liver metastasis and found a cancer-specific increase of sphingomyelin (SM) [22]. Ishikawa et al. found that phosphatidylcholine (PC), oleic acid, and SM were increased in the region of thyroid cancer, and proposed that these distributional differences were related to the biological behavior of cancer, for example invasion and metastasis [23]. Thus, IMS is a useful technique for finding and identifying specific molecules (especially lipids) in such pathology samples as cancer tissues. However, there has been no report of comparison of the signals in the cancer and stromal regions by use of IMS.

In this study, we attempted to find phospholipids specifically distributed in the cancer or stroma of OSCC tissue. Two consecutive tissue sections including cancer and stroma were prepared from OSCC tissue; one section was then analyzed by IMS and the other was stained with hematoxylin and eosin (HE). The mass range in IMS analysis was focused on phospholipids, and specific peaks in each cancer region and stromal region were analyzed by statistical analysis, by use of computer software. Molecules distributed differently between the cancer and stromal regions were visualized, and we determined whether each region was clearly distinguished. To identify these molecules, we conducted tandem mass spectrometric (MS/MS) analysis.

Materials and methods

Clinical samples

Gingival OSCC biopsy tissue blocks were obtained from five patients before surgery, in accordance with protocols approved by the Hamamatsu University School of Medicine. None of the patients had received radiation, chemotherapy, or immunotherapy treatment. Pathological examination was used to confirm these portions of tumor and the histology of invasive SCC. After they were obtained, the tissues blocks were immediately frozen in liquid nitrogen and stored at −80 °C to maintain tissue morphology and minimize molecular degradation until MALDI-IMS analysis.

Chemicals

Methanol, potassium acetate, and ultra-pure water were purchased from Wako Chemicals (Osaka, Japan). 2,5-Dihydroxybenzoic acid (DHB) was purchased from Bruker Daltonics (Bremen, Germany). Standard peptides for calibration of the TOF analyzer were purchased from Sigma–Aldrich (St Louis, MO, USA). All of the chemicals used in this study were of the highest purity available.

stromal regions. Phospholipids can be analyzed by IMS without complex treatment. This technique could simplify diagnosis and distinguish the regions by use of two phospholipids. All IMS and MS/MS experiments were performed using optimized settings, and the reproducibility of the data was evaluated by use of mass spectra acquired from adjacent sections.

The IMS analyses revealed statistically significant differences in intensity ($p<0.01$) for 11 peaks (Table 1) and the ion images characterized the stromal region or cancer region. Two signals at *m/z* 741 and *m/z* 798 were detected in cancer regions in other research by Shimma [22] and Ishikawa [23]. According to the ion image at *m/z* 741.5 in the study by Ishikawa et al., the distribution was a little different from that of other cancer-positive signals, for example *m/z* 796.5 and *m/z* 798.5. They mentioned that the signal at *m/z* 741.5 was more intense in both the cancer region and the stromal region. The signal at *m/z* 725.4 was also identified as SM (d18:1/16:0) with a different ion-adduct form. The ion image in the study by Shimma et al. also revealed greater intensity in the stromal region than in the cancer region. These results are identical with ours (Fig. 3). Even if a signal is evaluated as significantly different, signal which are extremely different should be used to distinguish the border between the cancer and stromal regions. Therefore, the signals at *m/z* 720.1, *m/z* 770.5, and *m/z* 794.5 for the cancer region and *m/z* 804.5, *m/z* 820.5, and *m/z* 846.6 for the stromal region were applied to all IMS datasets in this study (Fig. 5). These signals had good *p*-values in the statistical analysis (Table 1 and Fig. 4). The merged ion images of *m/z* 770.5 and *m/z* 846.6 revealed a clear border between the cancer and stromal regions without any of the overlap observed in the HE staining. In the near future, there is a possibility that these signals could be used as a diagnostic method to determine the resection area before surgery.

In this study, we successfully identified the signals at *m/z* 770.5 and *m/z* 846.6 as two PC species, i.e., PC (diacyl-16:0/16:1) in the cancer region and PC (diacyl-18:1/20:4) in the stromal region, from OSCC tissue sections (Fig. 6). Ishikawa et al. identified phospholipid species, for example PC (diacyl-16:0/18:1), PC (diacyl-16:1/18:1), and SM (d18:1/16:0), that were increased in the thyroid cancer region compared with the normal region [23]. In general, malignant cellular proliferation is stimulated by cell-growth factors, for example PC species, that are increased in the components of the cell membrane, with the increase in cell density. However, PC (diacyl-16:0/16:1) and PC (diacyl-18:1/20:4) have not been identified in the cancer and stromal regions. This suggests that each individual cancer cell has a different profile.

Here we focused on the fatty acid bound to PC species in OSCC cancer regions. The fatty acid compositions are also

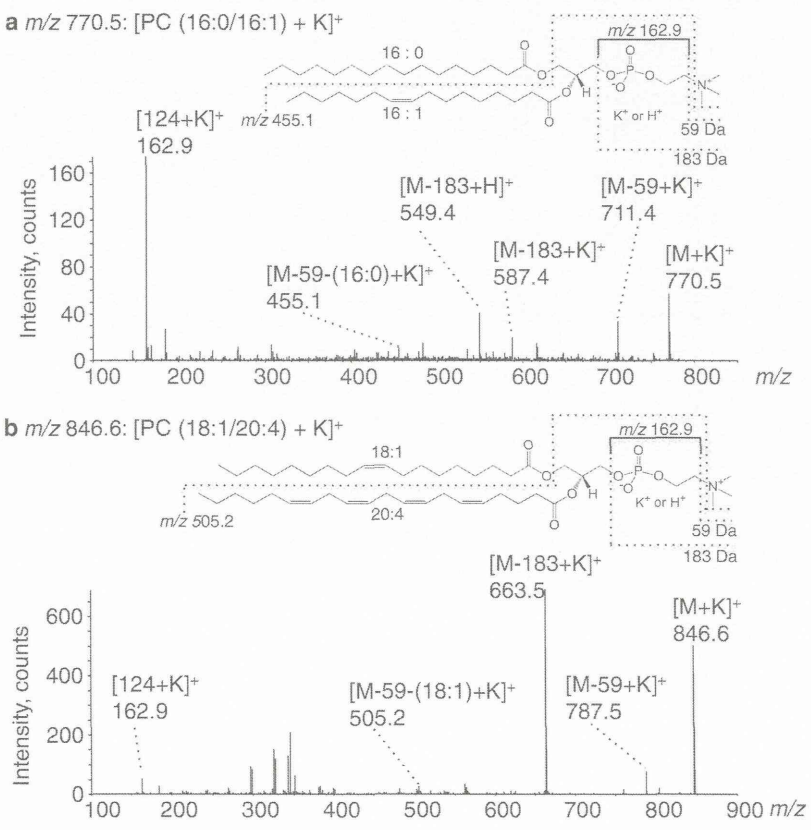

Fig. 6 Molecular identification by MS/MS analysis of tissue sections. Precursor ions were: *m/z* 770.5 (**a**) and *m/z* 846.6 (**b**). A molecule corresponding to *m/z* 770.5 was assigned by neutral loss as $[PC (16:0/16:1) + K]^+$. In the same manner, a molecule corresponding to *m/z* 846.6 was assigned as $[PC (18:1/20:4) + K]^+$

very interesting from the perspective of cancer invasion mechanisms. Lv et al. reported that the saturated fatty acids palmitic acid (C16:0) and stearic acid (C18:0) and the unsaturated fatty acid linoleic acid (C18:2) were increased in the serum of patients with breast cancer, and they proposed these fatty acids as new biomarkers of breast cancer [30]. Such an increase of fatty acids might reflect the synthesis of PC species including 16:0, 18:0, and 18:2. In fact, our results demonstrated that PC (diacyl-16:0/16:1) was increased in the cancer region of OSCCs.

In the HE-stained OSCC tissue section, many of the lymphocyte cells in the stromal region clearly had nuclei with different shapes compared with other cell types (Fig. 1c). It is well-known that lymphocyte cells accumulate in regions of inflammation [31], and histochemical analysis has revealed accumulation of immune lymphocytes in the stromal region of cervical cancer [32]. Hanada et al. reported that arachidonic acid (AA, 20:4) bound to PC species (AA-PCs) was detected in the inflammation region in a rat model of spinal cord injury. These results suggest that the PC (18:1/20:4) distributed in the OSCC stromal regions could have reflected an increase in cell membrane components induced by an accumulation of lymphocyte cells. Moreover, our results revealed an increase of signals at *m/z* 804.5 and *m/z* 820.5 in the stromal region. Previous reports showed that the signals at *m/z* 804.5 and *m/z* 820.5 were identified as PC (diacyl-16:0/20:4) [33] and PC (diacyl-16:1/20:4) [27, 34], respectively. Thus, three kinds of AA-PCs were increased in the stromal region, and there is a possibility that AA is important in tumor invasion in the stromal region.

AA is a precursor of prostaglandin (PG) and is converted by cyclooxygenase (COX) in the AA cascade. COX-1 is involved in the maintenance of homeostasis and in the constant supply of prostaglandin E2 (PGE2) [35]. COX-2 and the de-novo synthesis of the enzyme microsomal prostaglandin E synthase-1 (mPGES-1) are induced against the growth of tumor tissue, and this process also causes an increase of PGE2. PGE2 produced by COX-2 activation in the AA cascade in a stromal region is important in oncogenesis, initial tumorigenesis, and cancer cell differentiation in various histologic types, including OSCC [35–37]. Therefore, AAPCs identified as PC (diacyl-18:1/20:4) in a stromal region could be a source of lipid mediators of inflammation against cancer invasion.

In this study, we showed that PC (diacyl-16:0/16:1) was distributed in the cancer region. Such distributions in cancer regions have been reported by other researchers using IMS. Morita et al. reported the distribution of PC (diacyl-16:0/16:1) in hepatocellular carcinoma (HCC) [38]. Ide et al. revealed the distribution of PC (diacyl-32:1) in breast cancers but did not identify the fatty acid composition [39]. We speculate that the fatty acid composition could be diacyl-l6:0/16:1. Thus, according to results from OSCC, HCC, and breast cancer, PC species containing 16:0 are commonly distributed in the cancer region. On the other hand, Ishikawa et al. could not detect the signal at *m/z* 770.5 corresponding to PC (diacyl-16:0/16:1) in thyroid papillary cancers [23]. Therefore, each cancer should be carefully analyzed because of the different fatty acid components of PC species in the cancer region. Moreover, investigation of fatty acid synthesis by a fatty acid synthase and PC synthesis by lysophosphatidylcholine acyltransferase could elucidate the mechanism of proliferation, migration, and invasion in the cancer and stromal regions.

Conclusion

IMS analysis of OSCC tissue sections from one patient revealed eleven signals of significantly different intensities in the cancer and stromal regions. Two signals were specifically distributed in the cancer or stromal regions of the tissue sections from five patients. Therefore these signals, which were identified as those of PC (16:0/16:1) and PC (18:1/20:4) in the MS/MS analyses, could be used to distinguish the border between the cancer and stromal regions in OSCC.

Acknowledgments This study was supported in part by a Grant-in-Aid for Scientific Research (no. 22500406) from the Ministry of Education, Culture, Sports, Science, and Technology, Japan, by a Grant-in-Aid for Young Scientists (S) from the JSPS to MS, by a SENTAN grant from the Japan Science and Technology Agency, and by a Grant-in-Aid from the Ministry of Health, Labour and Welfare.

References

1. Jakobsson PA, Eneroth CM, Killander D et al (1973) Histologic classification and grading of malignancy in carcinoma of the larynx. Acta Radiol Ther Phys Biol 12(1):1–8
2. Anneroth G, Batsakis J, Luna M (1987) Review of the literature and a recommended system of malignancy grading in oral squamous cell carcinomas. Scand J Dent Res 95(3):229–249
3. Yamamoto E, Miyakawa A, Kohama G (1984) Mode of invasion and lymph node metastasis in squamous cell carcinoma of the oral cavity. Head Neck Surg 6(5):938–947
4. Nagata T, Schmelzeisen R, Mattern D et al (2005) Application of fuzzy inference to European patients to predict cervical lymph node metastasis in carcinoma of the tongue. Int J Oral Maxillofac Surg 34(2):138–142
5. Myoung H, Kim MJ, Lee JH et al (2006) Correlation of proliferative markers (Ki-67 and PCNA) with survival and lymph node metastasis in oral squamous cell carcinoma: a clinical and histopathological analysis of 113 patients. Int J Oral Maxillofac Surg 35(11):1005–1010
6. Kurokawa H, Zhang M, Matsumoto S et al (2005) The relationship of the histologic grade at the deep invasive front and the expression of Ki-67 antigen and p53 protein in oral squamous cell carcinoma. J Oral Pathol Med 34(10):602–607
7. Gschwind A, Prenzel N, Ullrich A (2002) Lysophosphatidic acid-induced squamous cell carcinoma cell proliferation and motility involves epidermal growth factor receptor signal transactivation. Cancer Res 62(21):6329–6336

8. Coussens LM, Werb Z (2002) Inflammation and cancer. Nature 420(6917):860–867
9. Guo Y, Wang X, Zhang X et al (2011) Ethanol promotes chemically induced oral cancer in mice through activation of the 5-lipoxygenase pathway of arachidonic acid metabolism. Cancer Prev Res (Phila) 4(11):1863–1872
10. Mann EA, Spiro JD, Chen LL et al (1994) Phospholipid metabolite expression by head and neck squamous cell carcinoma. Arch Otolaryngol Head Neck Surg 120(7):763–769
11. Brasitus TA, Dudeja PK, Dahiya R (1986) Premalignant alterations in the lipid composition and fluidity of colonic brush border membranes of rats administered 1,2 dimethylhydrazine. J Clin Invest 77(3):831–840
12. Setou M (2010) Imaging mass spectrometry: protocols for mass microscopy. Springer, New York
13. Gross JH (2004) Mass spectrometry: a textbook. Springer-Verlag, New York
14. Alexandrov T, Becker M, Guntinas-Lichius O et al (2013) MALDI-imaging segmentation is a powerful tool for spatial functional proteomic analysis of human larynx carcinoma. J Cancer Res Clin Oncol 139(1):85–95
15. Thomas A, Patterson NH, Marcinkiewicz MM et al (2013) Histology-driven data mining of lipid signatures from multiple imaging mass spectrometry analyses: application to human colorectal cancer liver metastasis biopsies. Anal Chem 85(5):2860–2866
16. Sugiura Y, Setou M (2010) Imaging mass spectrometry for visualization of drug and endogenous metabolite distribution: toward in situ pharmacometabolomes. J Neuroimmune Pharmacol 5(1):31–43
17. Joyner JC, Keuper KD, Cowan JA (2013) Analysis of RNA cleavage by MALDI–TOF mass spectrometry. Nucleic Acids Res 41(1):e2
18. Rubakhin SS, Hatcher NG, Monroe EB et al (2007) Mass spectrometric imaging of the nervous system. Curr Pharm Des 13(32):3325–3334
19. Jackson SN, Woods AS (2009) Direct profiling of tissue lipids by MALDI–TOFMS. J Chromatogr B Anal Technol Biomed Life Sci 877(26):2822–2829
20. Sugiura Y, Konishi Y, Zaima N et al (2009) Visualization of the cell-selective distribution of PUFA-containing phosphatidylcholines in mouse brain by imaging mass spectrometry. J Lipid Res 50(9):1776–1788
21. Schone C, Hofler H, Walch A (2013) MALDI imaging mass spectrometry in cancer research: combining proteomic profiling and histological evaluation. Clin Biochem 46(6):539–545
22. Shimma S, Sugiura Y, Hayasaka T et al (2007) MALDI-based imaging mass spectrometry revealed abnormal distribution of phospholipids in colon cancer liver metastasis. J Chromatogr B Anal Technol Biomed Life Sci 855(1):98–103
23. Ishikawa S, Tateya I, Hayasaka T et al (2012) Increased expression of phosphatidylcholine (16:0/18:1) and (16:0/18:2) in thyroid papillary cancer. PLoS One 7(11):e48873
24. Sugiura Y, Shimma S, Setou M (2006) Thin sectioning improves the peak intensity and signal-to-noise ratio in direct tissue mass spectrometry. J Mass Spectrom Soc Jpn 54:45–48
25. Schwartz SA, Reyzer ML, Caprioli RM (2003) Direct tissue analysis using matrix-assisted laser desorption/ionization mass spectrometry: practical aspects of sample preparation. J Mass Spectrom 38(7):699–708
26. Sugiura Y, Setou M (2009) Selective imaging of positively charged polar and nonpolar lipids by optimizing matrix solution composition. Rapid Commun Mass Spectrom 23(20):3269–3278
27. Enomoto H, Sugiura Y, Setou M et al (2011) Visualization of phosphatidylcholine, lysophosphatidylcholine and sphingomyelin in mouse tongue body by matrix-assisted laser desorption/ionization imaging mass spectrometry. Anal Bioanal Chem 400(7):1913–1921
28. Hayasaka T, Goto-Inoue N, Sugiura Y et al (2008) Matrix-assisted laser desorption/ionization quadrupole ion trap time-of-flight (MALDI–QIT-TOF)-based imaging mass spectrometry reveals a layered distribution of phospholipid molecular species in the mouse retina. Rapid Commun Mass Spectrom 22(21):3415–3426
29. Morita Y, Ikegami K, Goto-Inoue N et al (2010) Imaging mass spectrometry of gastric carcinoma in formalin-fixed paraffin-embedded tissue microarray. Cancer Sci 101(1):267–273
30. Lv W, Yang T (2012) Identification of possible biomarkers for breast cancer from free fatty acid profiles determined by GC–MS and multivariate statistical analysis. Clin Biochem 45(1–2):127–133
31. Aust S, Bachmayr-Heyda A, Pils D et al (2013) Determination of tumor-infiltrating CD8+ lymphocytes in human ovarian cancer. Int J Gynecol Pathol 32(3):269–276
32. Bedoya AM, Jaramillo R, Baena A et al (2012) Location and density of immune cells in precursor lesions and cervical cancer. Cancer Microenviron 6(1):69–77
33. Tanaka H, Zaima N, Yamamoto N et al (2011) Distribution of phospholipid molecular species in autogenous access grafts for hemodialysis analyzed using imaging mass spectrometry. Anal Bioanal Chem 400(7):1873–1880
34. Hanada M, Sugiura Y, Shinjo R et al (2012) Spatiotemporal alteration of phospholipids and prostaglandins in a rat model of spinal cord injury. Anal Bioanal Chem 403(7):1873–1884
35. Gupta RA, Dubois RN (2001) Colorectal cancer prevention and treatment by inhibition of cyclooxygenase-2. Nat Rev Cancer 1(1):11–21
36. Zhang S, Du Y, Tao J et al (2008) Expression of cytosolic phospholipase A2 and cyclooxygenase 2 and their significance in human oral mucosae, dysplasias and squamous cell carcinomas. ORL J Otorhinolaryngol Relat Spec 70(4):242–248
37. Shibata M, Kodani I, Osaki M et al (2005) Cyclo-oxygenase-1 and -2 expression in human oral mucosa, dysplasias and squamous cell carcinomas and their pathological significance. Oral Oncol 41(3):304–312
38. Morita Y, Sakaguchi T, Ikegami K et al (2013) Lysophosphatidylcholine acyltransferase 1 altered phospholipid composition and regulated hepatoma progression. J Hepatol in press
39. Ide Y, Waki M, Hayasaka T et al (2013) Human breast cancer tissues contain abundant phosphatidylcholine(36:1) with high stearoyl-CoA desaturase-1 expression. PLoS One 8(4):e61204

OPEN ACCESS Freely available online

PLOS ONE

Human Breast Cancer Tissues Contain Abundant Phosphatidylcholine(36:1) with High Stearoyl-CoA Desaturase-1 Expression

Yoshimi Ide[1,2☯], Michihiko Waki[2☯], Takahiro Hayasaka[2], Tomohisa Nishio[3], Yoshifumi Morita[2], Hiroki Tanaka[2], Takeshi Sasaki[4], Kei Koizumi[1], Ryoichi Matsunuma[1], Yuko Hosokawa[1], Hiroyuki Ogura[1], Norihiko Shiiya[1], Mitsutoshi Setou[2]*

1 Department of Surgery I, Hamamatsu University School of Medicine, Hamamatsu, Japan, **2** Department of Cell Biology and Anatomy, Hamamatsu University School of Medicine, Hamamatsu, Japan, **3** Department of Laboratory Medicine, Hamamatsu University School of Medicine, Hamamatsu, Japan, **4** Department of Anatomy and Neuroscience, Hamamatsu University School of Medicine, Hamamatsu, Japan

Abstract

Breast cancer is the leading cause of cancer and mortality in women worldwide. Recent studies have argued that there is a close relationship between lipid synthesis and cancer progression because some enzymes related to lipid synthesis are overexpressed in breast cancer tissues. However, lipid distribution in breast cancer tissues has not been investigated. We aimed to visualize phosphatidylcholines (PCs) and lysoPCs (LPCs) in human breast cancer tissues by performing matrix assisted laser desorption/ionization-imaging mass spectrometry (MALDI-IMS), which is a novel technique that enables the visualization of molecules comprehensively. Twenty-nine breast tissue samples were obtained during surgery and subjected to MALDI-IMS analysis. We evaluated the heterogeneity of the distribution of PCs and LPCs on the tissues. Three species [PC(32:1), PC(34:1), and PC(36:1)] of PCs with 1 mono-unsaturated fatty acid chain and 1 saturated fatty acid chain (MUFA-PCs) and one [PC(34:0)] of PCs with 2 saturated fatty acid chains (SFA-PC) were relatively localized in cancerous areas rather than the rest of the sections (named reference area). In addition, the LPCs did not show any biased distribution. The relative amounts of PC(36:1) compared to PC(36:0) and that of PC(36:1) to LPC(18:0) were significantly higher in the cancerous areas. The protein expression of stearoyl-CoA desaturase-1 (SCD1), which is a synthetic enzyme of MUFA, showed accumulation in the cancerous areas as observed by the results of immunohistochemical staining. The ratios were further analyzed considering the differences in expressions of the estrogen receptor (ER), human epidermal growth factor receptor 2 (HER2), and Ki67. The ratios of the signal intensity of PC(36:1) to that of PC(36:0) was higher in the lesions with positive ER expression. The contribution of SCD1 and other enzymes to the formation of the observed phospholipid composition is discussed.

Citation: Ide Y, Waki M, Hayasaka T, Nishio T, Morita Y, et al. (2013) Human Breast Cancer Tissues Contain Abundant Phosphatidylcholine(36:1) with High Stearoyl-CoA Desaturase-1 Expression. PLoS ONE 8(4): e61204. doi:10.1371/journal.pone.0061204

Editor: Francisco X. Real, Centro Nacional de Investigaciones Oncológicas (CNIO), Spain

Received December 5, 2012; **Accepted** March 6, 2013; **Published** April 16, 2013

Copyright: © 2013 Ide et al. This is an open-access article distributed under the terms of the Creative Commons Attribution License, which permits unrestricted use, distribution, and reproduction in any medium, provided the original author and source are credited.

Funding: This study was supported by grants-in-aid for the scientific research project "Machinery of bioactive lipids in homeostasis and diseases" from the Ministry of Education, Culture, Sports, Science and Technology of Japan and Health Labor Sciences Research Grant from a Ministry of Health, Labor and Welfare. The funders had no role in study design, data collection and analysis, decision to publish, or preparation of the manuscript.

Competing Interests: The authors have declared that no competing interests exist.

* E-mail: setou@hama-med.ac.jp

☯ These authors contributed equally to this work.

Introduction

Breast cancer is the leading cause of cancer and cancer related mortality in women worldwide [1]. Recently, the activation of lipid metabolism in breast cancer cells has been increasingly recognized as a hallmark of carcinogenesis [2,3]. In particular, phosphatidylcholines (PCs) are generally the most abundant phospholipid species in mammalian cells, and PC synthesis and metabolism in cancer progression have been investigated [4]. Aberrancy in PC metabolism, which is mainly through the increased degradation of PCs, was indicated in a study using nuclear magnetic resonance for the analysis of breast cancer cell lines; however, they did not distinguish the acyl chain structures of the PCs [5–7]. The characterization of breast cancer tissues from patients by differentiating among molecular species of PCs has been reported by using gas chromatography [8] and liquid chromatography/mass spectrometry [9]. Biomarker investigation by lipidomic analysis including several PC species has been proposed for several PC species as putative diagnostic markers and therapeutic targets [9].

In this report, we apply matrix assisted laser desorption/ionization (MALDI)-imaging mass spectrometry (IMS), which is a recently developed analysis methodology [10], to analyze breast cancer tissues. MALDI-IMS enables biomolecules on tissue samples to be ionized while preserving their positional information by 2-dimensional laser scanning. The ionized biomolecules can be simultaneously analyzed by using a time-of-flight type mass spectrometer and identified according to their mass-to-charge ratio (m/z). The distribution of a target biomolecule is 2-

dimensionally visualized as the relative ratio of the signal intensity among the measurement points of the tissue section [11–13].

Herein, we mainly visualize some specific PCs composed of mono-unsaturated fatty acids (MUFAs) and saturated fatty acids (SFAs), since the incorporation of these fatty acid into PCs and the proportion of the PCs as end products in cancer cells are not well understood. Stearoyl-CoA desaturase-1 (SCD1) is a microsomal enzyme that regulates the conversion of SFA (palmitic [16:0] and stearic acid [18:0]) into MUFA (palmitoleic [16:1] and oleic acid [18:1], respectively) [14–16] (Figure 1) and is suggested to play an important role in cancer progression [17]. Although a recent study has proposed that higher SCD1 expression is a poor prognostic marker for breast cancer [18], reports on the use of immunohistochemical analysis using human breast cancer tissues are limited [19]. Therefore, we examine SCD1 expression and its correspondence with the composition of phospholipids as the final products of sequential enzymatic reactions, including desaturation.

In this report, we attempt to visualize phospholipids in breast cancer tissues, and describe the distributions by means of signal intensities of the molecules and the ratios by discriminating the area containing cancer cells and the rest of the sections. We evaluate the expression of SCD1 proteinin cancer cells to consider the relationship between desaturation and lipid composition. Lipid composition is further analyzed with regard to estrogen receptor (ER), human epidermal growth factor receptor 2 (HER2), and Ki67 expression.

Methods

Ethics Statement

All the experiments in this study were specifically approved by the Ethics Committee at the Hamamatsu University School of Medicine. Informed consent was obtained in written form from each patient before performing each operation. One patient under 20 years of age was involved in our study and for her informed consent was obtained in written form from her parents as well. The subjects consented to cooperate after they were informed that they would not incur any disadvantage, that they could resign from the study, that the researchers were obliged to protect their privileged information, and that their identities would not be revealed.

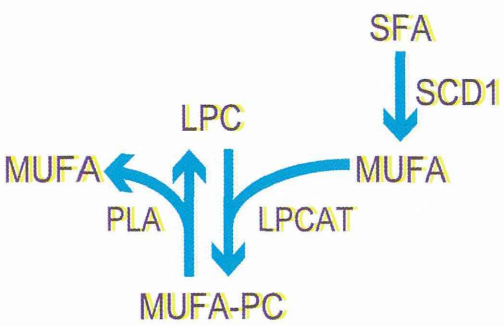

Figure 1. Pathway for synthesizing MUFA-PCs catalyzed by LPCAT and LPC. Endogenously synthesized mono-unsaturated fatty acids (MUFAs) are converted from saturated fatty acids (SFA) by the catalyzing effect of stearoyl-CoA desaturase-1 (SCD1). A MUFA is added to a lyso-phosphatidylcholine (LPC) through lysophosphatidylcholine acyltransferase (LPCAT) to produce a phosphatidylcholine (PC) that contains MUFA (MUFA-PC). A MUFA-PC is degraded to a LPC and a MUFA by phospholipase A1 (PLA1) and PLA2.
doi:10.1371/journal.pone.0061204.g001

Subjects

Tissue samples were obtained from 29 patients (sample No. 1–29; n = 29), who underwent surgery at our hospital (University Hospital, Hamamatsu University School of Medicine). Only 1 sample (sample No. 20) was from a breast fibroadenoma that had been resected from a patient who did not have cancer, while the other 28 samples (No. 1 to 29 except 20) were resected from patients who had been diagnosed with breast cancer on the basis of pathological examinations by using formalin fixed and paraffin embedded (FFPE) tissue sections. All of the samples in this study were reexamined microscopically by 2 authors (YI and HO). Since 1 out of 28 samples that were obtained from cancer patients did not contain any cancer cells (sample No. 28), 27 samples were used for the analysis of cancer lesions. All of the patients were Japanese women who were aged 16–87 y (mean age, 59.3 y). One out of the 28 breast cancer patients received preoperative systemic therapy (sample No. 10). Three out of the 28 patients had non-invasive ductal carcinomas (sample No. 3, 18, and 24) and the others had invasive carcinomas.

Information on the expression of ER, HER2, and Ki67 was also obtained from the pathological records of clinical specimen in the patients' medical records. Specimens showing positive staining for ER in >10% of the total cancer cells were defined as being positive ER lesions (sample No. 2, 3, 6–9, 11, 13–18, 22–27, and 29; n = 20). The others were classified into negative ER lesions (sample No. 1, 4, 5, 10, 12, 19, and 21; n = 7). HER2 positivity was determined according to the guidelines of the American Society of Clinical Oncology and the College of American pathologists [20]. Tumor cells with cell membranes that were completely stained by HER2 antibody comprising of >30% of the total cancer cells were given an HER2 scoring of 3+ and recognized as being HER2 positive lesions. A fluorescence in situ hybridization test was performed for the lesions with HER2 scores of 2+ and lesions with a signal ratio of over 2.2 were recognized as being HER2 positive (sample No. 1, 8, 11, 12, 19, and 22; n = 6). The other lesions were considered as being HER2 negative (sample No.2–7, 9, 10, 13–18, 21, 23–27, and 29; n = 21). Seventeen of the patients were ER and/or progesterone receptor (PgR) positive and HER2 negative (sample No. 2, 3, 6–9, 11, 13–18, 22–27, and 29; n = 17), 3 were ER and/or PgR positive and HER2 positive (sample No. 8, 11, and 22; n = 3), 3 were both ER and PgR negative and HER2 positive (sample No. 1, 12, and 19; n = 3), and 4 were triple negative (sample No. 4, 5, 10, and 21; n = 4). Lesions with a Ki67 index of over 20% were recognized as belonging to the higher Ki67 group and fewer than 20% belonged to the lower group [21]. Information on the Ki67 labeling index of 21 out of the 27 lesions was obtained from medical records; 14 lesions (sample No. 2, 3, 6, 7, 9, 10, 13, 16, 18, 24–27, and 29; n = 14) were classified as belonging to the lower Ki67, and 7 belonged to the higher Ki67 (sample No. 4, 5, 8, 11, 12, 15, and 17; n = 7).

Chemicals

Calibration standard peptides (Bradykinin fragment 1–7 and Angiotensin II) and 2, 5-dihydroxybenzoic acid (DHB) were purchased from Sigma-Aldrich (St. Louis, MO, USA).

Sample Preparation

Samples for analysis by IMS were immediately frozen in liquid hexanes to minimize degradation and were kept at −80°C. The specimens were sliced into 10-μm thick sections using a cryostat (CM1950; Leica, Wetzler, Germany). During sectioning, the temperature in the cryostat was maintained at −20°C. Then, the slices that were to be used for MALDI-IMS were mounted onto indium-tin-oxide (ITO)-coated glass slides (Bruker Daltonics,